NANO LETTERS

pubs.acs.org/NanoLett Letter

CRISPR-Guided Programmable Self-Assembly of Artificial Virus-Like Nucleocapsids

Carlos Calcines-Cruz, Ilya J. Finkelstein,* and Armando Hernandez-Garcia*

Cite This: https://doi.org/10.1021/acs.nanolett.0c04640 Read Online

ACCESS | Metrics & More | Article Recommendations | Supporting Information

ABSTRACT: Designer virus-inspired proteins drive the manufacturing of more effective, safer gene-delivery systems and simpler models to study viral assembly. However, self-assembly of engineered viromimetic proteins on specific nucleic acid templates, a distinctive viral property, has proved difficult. Inspired by viral packaging signals, we harness the programmability of CRISPR-Cas12a to direct the nucleation and growth of a self-assembling synthetic polypeptide into virus-like particles (VLP) on specific DNA molecules. Positioning up to ten nuclease-dead Cas12a (dCas12a) proteins along a 48.5 kbp DNA template triggers particle growth and full DNA encapsidation at limiting polypeptide concentrations. Particle growth rate is further increased when dCas12a is dimerized with a polymerization silk-like domain. Such improved self-assembly efficiency allows for discrimination between cognate versus noncognate DNA templates by the synthetic polypeptide. CRISPR-guided VLPs will help to develop programmable bioinspired nanomaterials with applications in biotechnology as well as viromimetic scaffolds to improve our understanding of viral self-assembly.

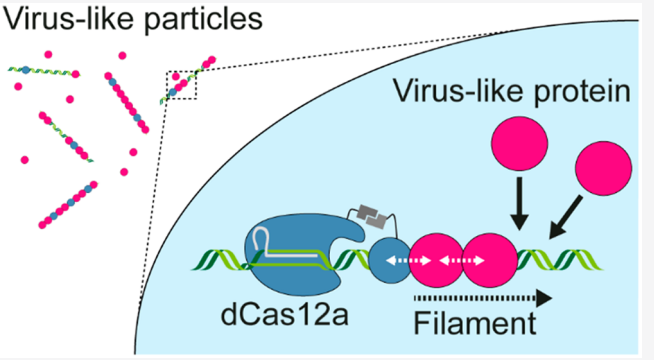

KEYWORDS: *virus-like particles, Cas12a, assembly kinetics, DNA curtain*

Virus-like particles (VLPs) mimic the capability of some viruses to encapsulate and protect genetic material from degradation by nucleases. We have previously described VLPs formed by the self-assembly of a triblock polypeptide (C−S_{10}−B) that functionally mimics the tobacco mosaic virus coat protein[1] (Figure 1a, Figure S1). C−S_{10}−B fuses three independent blocks: (1) "C" (∼400 aa), a random coil collagen-like domain that consists mostly of glycine, proline, and uncharged polar amino acids;[2] (2) "S_{10}", a silk-inspired polymerization domain with the sequence $[(AG)_3QG]_{10}$ that is responsible for C−S_{10}−B self-assembly into rodlike structures;[3−5] and (3) "B", a cationic dodecalysine stretch that interacts with nucleic acids and other polyanions.[6,7] C−S_{10}−B nucleates (without sequence specificity) on double-stranded DNA (dsDNA), albeit with a preference for free DNA ends.[8] After rate-limiting nucleation, C−S_{10}−B filaments grow rapidly through elongation,[1,9] similar to the assembly of the tobacco mosaic virus coat protein on genomic ssRNA.

Viral coat proteins preferentially encapsulate their own genomes. They achieve such specificity by encoding one or more packaging signals along the viral DNA or RNA. These sequences bind capsid proteins with high affinity[10−17] and decrease the energy barrier for nucleation, thereby promoting encapsidation of the viral genome among a vast excess of cellular nucleic acids.[18−21] We reasoned that designer VLPs can also leverage a similar packaging signal to enhance nucleation at specific DNA sites. We chose the catalytically dead CRISPR-Cas12a (dCas12a) as a programmable nucleation signal because it binds dsDNA with 50 fM affinity, has a higher DNA binding specificity than *S. pyogenes* Cas9,[22] and can be directed to multiple sites along the DNA via pooled CRISPR RNAs (crRNAs).[23]

Self-assembly kinetics were monitored in real-time using the single-molecule DNA curtain assay (Figure 1b).[24,25] For this, arrays of DNA molecules (48.5 kbp, derived from λ-phage) are affixed to a lipid bilayer via a biotin−streptavidin linkage in a microfluidic flowcell. Microfabricated chromium barriers are used to organize thousands of DNA strands for high-throughput data collection and analysis. The surface-immobilized DNA is extended for fluorescent imaging via the application of mild buffer flow. DNA length was monitored in the experiment because time-dependent DNA contraction is a direct readout of VLP filamentation (Figure 1c).[1]

First, we identified the minimal concentrations for efficient encapsidation of individual dsDNA substrates by C−S_{10}−B alone. At 100−300 nM, C−S_{10}−B monotonically condensed

Received: November 23, 2020
Revised: March 11, 2021

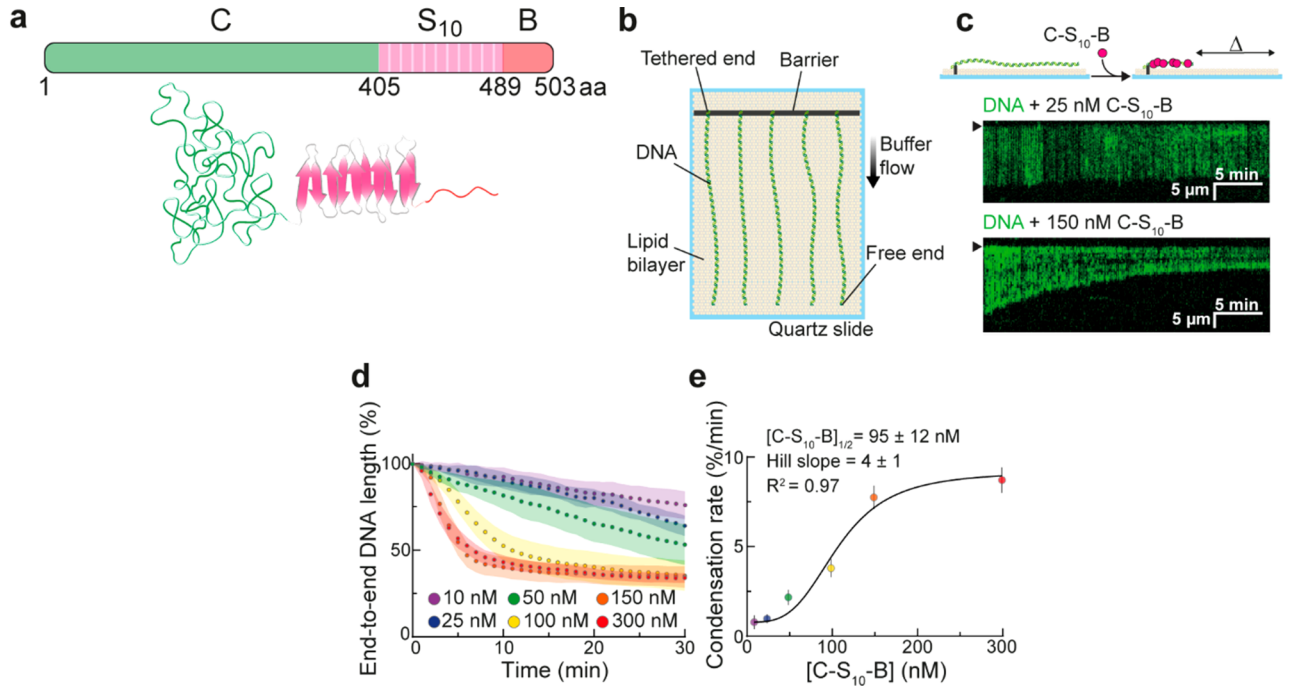

Figure 1. Synthetic polypeptide C−S_{10}−B packages DNA into nucleocapsids via molecular self-assembly. (a) Schematic depiction and modular design of C−S_{10}−B. (b) Illustration of the DNA curtain assay. Individual DNA molecules are captured on the surface of a lipid bilayer-passivated flowcell and extended by gentle buffer flow. (c) Representative kymographs showing condensation of individual DNA strands (green) at different rates determined by C−S_{10}−B concentration. The DNA is stained with the intercalating dye YOYO-1. Barrier position is indicated with black arrows on the kymographs. (d) DNA condensation profiles at the indicated C−S_{10}−B concentrations. The circles and shaded areas represent the mean and standard deviation for 25 molecules per condition, respectively. (e) DNA condensation rate in the first 3 min of assembly at different concentrations of C−S_{10}−B. The data were fit to the Hill equation (solid line). Circles and error bars are the mean ±95% confidence intervals for 25 DNA molecules per condition.

individual DNA molecules until complete assembly of linear particles with a final length of 34 ± 3% of the initial length (N = 25 DNA molecules at each concentration) (Figure 1d). Total DNA contraction to about one-third of the DNA original length has also been observed by previous AFM studies.[1] The DNA encapsidation rate—measured as t_{half}, the time required to achieve half of total packaging—decreased with higher C−S_{10}−B concentrations up to 50 nM and plateaued at [C−S_{10}−B] ≥ 100 nM (Figure S2a). In addition, the DNA did not completely contract at [C−S_{10}−B] ≤ 50 nM as compared to 100−300 nM. Together, these observations indicate incomplete C−S_{10}−B coating of the DNA at ≤50 nM C−S_{10}−B concentrations. Initial condensation rate increased with C−S_{10}−B concentration in a sigmoid-shaped curve distinctive of nucleated self-assemblies (Figure 1e). DNA coating was significantly impaired at 25 nM C−S_{10}−B compared with 150 nM (Figure S2b, c). These results are consistent with a dynamic equilibrium between C−S_{10}−B nucleation-filamentation and dissociation from DNA, akin to RAD51 and other dynamic filaments.[26]

Next, we evaluated whether positioning dCas12a on the DNA can improve encapsidation at low C−S_{10}−B concentrations. The DNA was uniformly decorated with five or ten dCas12a-crRNA ribonucleoproteins (RNPs) (Figure 2a). We confirmed site-specific target binding by imaging fluorescent RNPs along the DNA molecule (Figure S3a, b). We observed 1−4 target-bound RNPs on DNA substrates harboring five binding sites (1.2 ± 0.5 RNP per DNA, N = 456 DNA molecules) and 1−7 RNPs on DNA substrates with ten binding sites (2.6 ± 1.1 RNP per DNA, N = 185 DNA molecules) (Figure S3c). Because not all RNPs are decorated with fluorescent QDs, our results are a lower bound on the true target site occupancy. To monitor how encapsidation varies with RNP density, we injected 25 nM C−S_{10}−B into flowcells where the DNA was predecorated with either five or ten RNPs (Figure 2b, c). DNA contraction rate increased 2- and 3-fold for DNA with five (t_{half} = 15 ± 7 min; N = 25 DNA molecules) and ten (t_{half} = 10 ± 3 min; N = 25 DNA molecules) RNPs with respect to nondecorated DNA (t_{half} = 31 ± 6 min; N = 25 DNA molecules) (Figure 2d). We conclude that dCas12a RNPs can be installed at specific sites along the DNA template to accelerate encapsidation by C−S_{10}−B.

We reasoned that dCas12a organizes large C−S_{10}−B clusters that further polymerize into filaments. Two-color imaging confirmed that fluorescent C−S_{10}−B colocalizes with the RNPs at early stages of encapsidation (Figure 2e). Positioning five RNPs on the DNA increased the number of fluorescent C−S_{10}−B puncta per DNA strand from 1−3 (1.3 ± 0.6, N = 166 DNA molecules) to 2−7 (3.3 ± 1.0, N = 97 DNA molecules) for DNA and dCas12a-decorated DNA, respectively (Figure 2f). C−S_{10}−B protomers can freely diffuse on the DNA.[27] In the presence of buffer flow, these molecules slide and assemble into large clusters at the free DNA ends. In contrast, C−S_{10}−B accumulated at dCas12a sites on the decorated DNA (Figure S3d). C−S_{10}−B binding was also more rapid on predecorated DNA substrates (t_{half} = 15 ± 6 min; N = 10 DNA molecules) than on nondecorated DNA (t_{half} = 45 ± 15 min; N = 10 DNA molecules) (Figure 2g, h). C−S_{10}−B filamentation was unable to displace dCas12a, which forms a stable RNA:DNA loop (R-loop) with the DNA substrate (Figure S3e). Because dCas12a may act as a roadblock for C−S_{10}−B linear diffusion on the DNA, we also tested whether other DNA-binding proteins will accumulate C−S_{10}−B clusters. Notably, DNA decoration with nucleosomes also accelerated DNA encapsidation and particle

https://doi.org/10.1021/acs.nanolett.0c04640
Nano Lett. XXXX, XXX, XXX−XXX

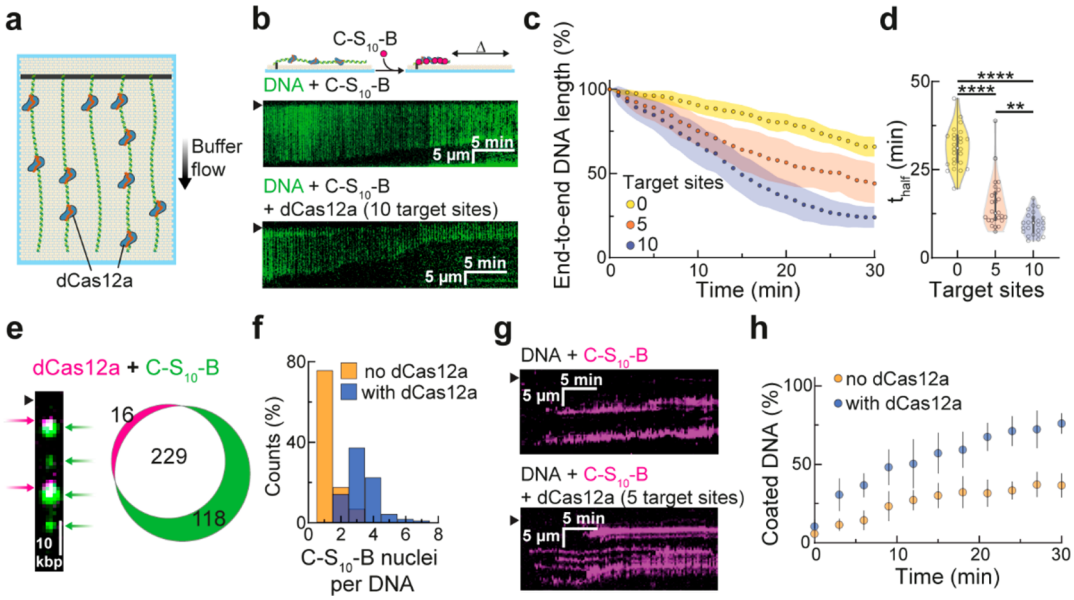

Figure 2. Seeding assembly with dCas12a improves DNA encapsidation by C−S_{10}−B. (a) Illustration of dCas12a-decorated DNA substrates. dCas12a is incubated with pools of crRNAs and directed to five or ten sites uniformly distributed along the DNA prior to C−S_{10}−B injection. (b) Representative kymographs show faster encapsidation at 25 nM C−S_{10}−B after the DNA (green) is decorated with dCas12a. Barrier position is indicated with arrows on the kymographs. (c) Condensation profiles at 25 nM C−S_{10}−B for DNA, and DNA decorated with dCas12a targeting five or ten sequences along the template. The circles and shaded areas represent the mean and standard deviation for 25 molecules per condition, respectively. (d) Violin plots showing the time (t_{half}) required to reach half of maximum condensation for each DNA molecule analyzed in panel c. We extrapolated t_{half} (after curve fitting to the Hill equation) for molecules that did not reach 66.5% encapsidation during the experiment (30 min). (**) and (****) indicate $p < 0.01$ and $p < 0.0001$, respectively. (e) Double labeling experiments show that 93% of dCas12a (magenta) colocalized with 66% of fluorescent C−S_{10}−B clusters (green). Barrier position is indicated with a black arrow. (f) Positioning five dCas12a on the DNA increases the number of fluorescent C−S_{10}−B clusters relative to undecorated DNA (N = 484 and 246 clusters, respectively). (g) Kymographs showing binding of C−S_{10}−B (magenta) on undecorated (top) or dCas12a-decorated (bottom) DNA (unlabeled) at 25 nM C−S_{10}−B. Barrier position is indicated with black arrows on the kymographs. (h) Extent of DNA that is coated by fluorescent C−S_{10}−B. Points and error bars indicate the mean and standard deviation, respectively (N = 10 DNA molecules per condition).

growth (Figure S4). We conclude that dCas12a stalls C−S_{10}−B sliding on DNA, which enhances C−S_{10}−B collisions in its vicinity and triggers particle nucleation. In support of this model, Marchetti et al.[27] observed that immobile C−S_{10}−B clusters, and not their sliding counterparts, initiate filament growth.

To further promote and accelerate DNA packaging at limiting C−S_{10}−B concentrations, we physically coupled dCas12a to the diblock polypeptide C−S_{10} via the rapamycin-inducible dimerization of FKBP and FRB domains (Figure 3a). We cloned and purified a dCas12a$_{(FKBP)}$ C-terminal fusion and verified that this construct retains target-specific DNA binding (Figure S5). The FRB domain was fused to a truncated C−S_{10} polypeptide that lacks the "B" DNA-binding module. Both proteins, dCas12a$_{(FKBP)}$ and C−$S_{10(FRB)}$, were incubated with rapamycin and the dimerized complex was injected into the flowcell prior to incubation with 10 nM C−S_{10}−B (Figure 3b, c). Positioning five dimerized dCas12a-S_{10} complexes along the DNA substrate accelerated encapsidation by C−S_{10}−B 2-fold relative to dCas12a$_{(FKBP)}$ alone (t_{half} = 9 ± 3 min; N = 25 DNA molecules vs 18 ± 6 min; N = 25 DNA molecules), and 5-fold relative to the undecorated DNA (t_{half} = 46 ± 13 min; N = 25 DNA molecules) (Figure 3d, e). Positioning dCas12a-S_{10} on a 2.5 kbp linear dsDNA or a 9.5 kbp plasmid also improved encapsidation at limiting C−S_{10}−B concentrations in ensemble electrophoretic mobility shift assays (EMSAs) (Figure S6). These results indicate that initiating nucleation via interspersed dCas12a RNPs fused to the self-assembly domain S_{10} accelerates DNA packaging at subsaturating C−S_{10}−B concentrations. Importantly, decoration with dCas12a or dCas12a-S_{10} did not disrupt the morphology of the artificial nucleocapsids, and full particles of 1/3 of the template DNA length were observed by AFM (Figure S7).

Finally, we assessed whether targeting dCas12a-S_{10} to a specific DNA template can trigger VLP encapsidation in the presence of other (noncognate) DNA molecules. For this assay, we immobilized an equimolar mixture of two DNA templates on the flowcell surface; one was 20 kbp and the second was 28.5 kbp (Figure 4a). dCas12a-S_{10} was directed to 5, 10, or 25 sites on the 28.5 kbp template (Figure 4b). As seen in Figure 4c, d and Figure S8, dCas12a-S_{10} selectively accelerated the packaging of the target DNA template and the encapsidation rate increased 3-fold from zero target sites (t_{half} = 62 ± 26 min; N = 25 DNA molecules) to a maximum of 25 target sites (t_{half} = 19 ± 6 min; N = 25 DNA molecules).

Taken together, our data show that a target DNA-bound dCas12a (or any strongly DNA-bound roadblock protein) can serve as a viral-like packaging signal—especially if the roadblock protein contains a self-assembly or polymerization domain. RNA-guided CRISPR-Cas proteins are especially attractive as artificial packaging signals because they can be targeted to any DNA sequence that is proximal to a protospacer adjacent motif (PAM). For *As*dCas12a, the PAM consensus sequence is TTTV; this PAM appears on average every 32 bp on 48.5 kbp long λ-phage DNA. Other CRISPR-Cas enzymes, including Cas9, can also serve as nucleation signals. Relaxed PAM variants, both for Cas9 and Cas12a, will further increase the targeting possibilities for rapid and sequence specific VLP assembly.[28−31]

https://doi.org/10.1021/acs.nanolett.0c04640
Nano Lett. XXXX, XXX, XXX−XXX

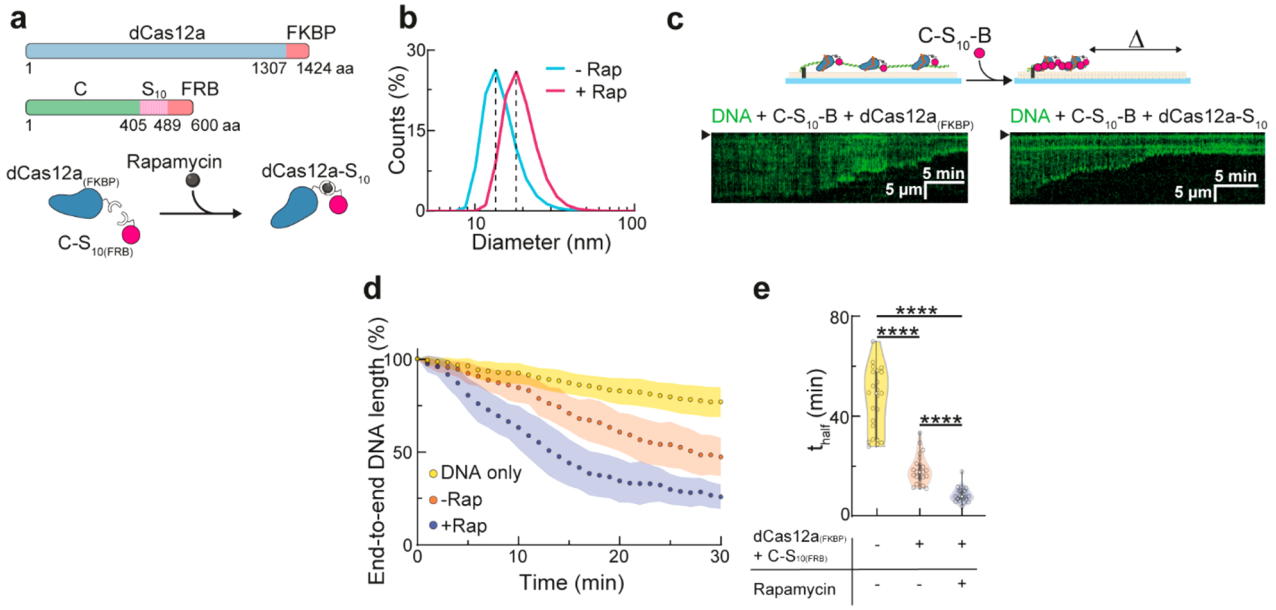

Figure 3. Coupling of dCas12a to the polymerization domain C−S_{10} improves C−S_{10}−B self-assembly on DNA. (a) Schematic depiction of the modular design of $dCas12a_{(FKBP)}$ and C−$S_{10(FRB)}$ and their dimerization via rapamycin to form the dCas12a-S_{10} complex. (b) Dynamic light scattering experiment showing rapamycin (Rap) induced dimerization of $dCas12a_{(FKBP)}$ and C−$S_{10(FRB)}$. The shift in population size occurred immediately after rapamycin addition. (c) Representative kymographs showing that decorating DNA with dCas12a-S_{10} accelerates DNA packaging relative to decoration with $dCas12a_{(FKBP)}$ alone at 10 nM C−S_{10}−B. Barrier position is indicated with arrows on the kymographs. (d) Condensation profiles at 10 nM C−S_{10}−B for undecorated DNA, and DNA decorated with five $dCas12a_{(FKBP)}$ or five dCas12a-S_{10}. The circles and shaded areas represent the mean and standard deviation for 25 molecules per condition, respectively. (e) Violin plots showing the time (t_{half}) required to reach half of maximum condensation for each DNA strand analyzed in panel d. Extrapolation (after curve fitting to the Hill equation) was used to estimate t_{half} for molecules that did not reach 66.5% encapsidation during the experiment (30 min). (****) indicates $p < 0.0001$.

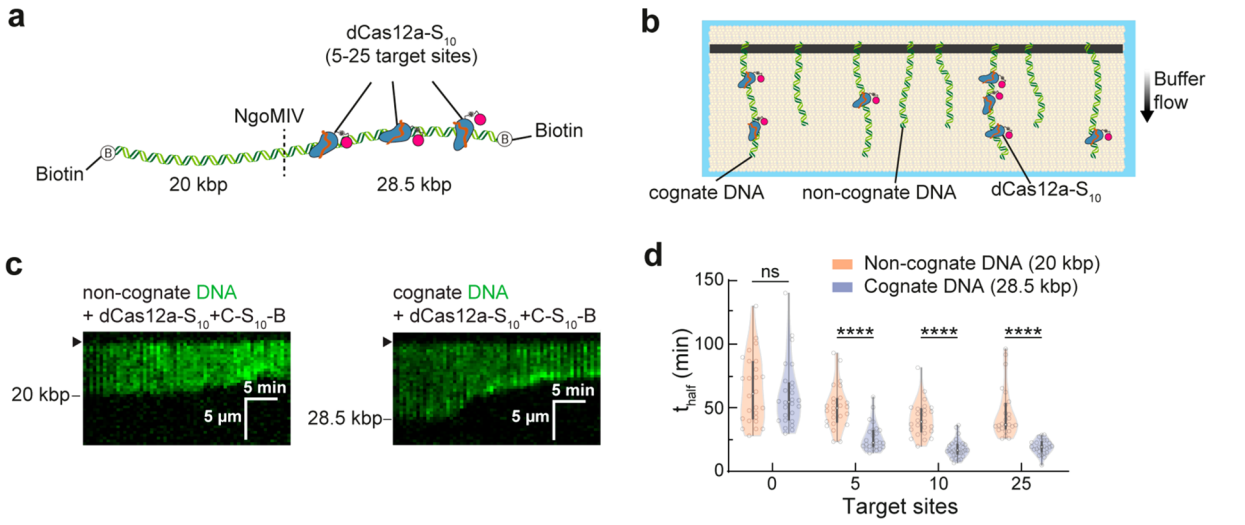

Figure 4. C−S_{10}−B selectively assembles on DNA that is decorated with dCas12a-S_{10}. (a) DNA was ligated with biotinylated oligos at both ends followed by cleavage with NgoMIV to generate two biotinylated DNA substrates (20 kbp and 28.5 kbp) distinguishable by size after YOYO-1 staining. (b) 28.5 kbp DNA (cognate DNA) was decorated with 5 to 25 dCas12a-S_{10} prior to incubation with 10 nM C−S_{10}−B. (c) Representative kymographs showing encapsidation of the noncognate (20 kbp) and cognate (28.5 kbp) DNA substrates after decoration with ten dCas12a-S_{10}. Barrier position is indicated with arrows on the kymographs. (d) Violin plots showing the time (t_{half}) required to reach half of maximum condensation for both DNA substrates after decoration of the cognate DNA with 5 to 25 dCas12a-S_{10}. Extrapolation (after curve fitting to the Hill equation) was used to estimate t_{half} for molecules that did not reach 66.5% encapsidation during the experiment (30 min). (ns) and (****) indicate $p > 0.05$ and $p < 0.0001$, respectively.

Additionally, this work shows that the C−S_{10}−B protein can be re-engineered to more closely resemble virus-like features.

In summary, we have used CRISPR-dCas12a and coupled it to the polymerization domain S_{10} to form a "packaging signal recognition complex" (in analogy with the assembly of viral capsid proteins around the viral genome) that triggers binding of C−S_{10}−B and packaging of target DNA sequences. Importantly, such packaging signal recognition complex (and hence artificial particle nucleation and growth) can be easily redirected toward different DNA sequences by simple design of the crRNA without need of the more cumbersome manipulation of protein domains. Moreover, our results highlight the importance of

https://doi.org/10.1021/acs.nanolett.0c04640
Nano Lett. XXXX, XXX, XXX−XXX

having multiple strong and specific interactions in templated nucleoprotein self-assemblies and should prove useful for developing new tailor-made nanomaterials for diverse biotechnological applications.

■ ASSOCIATED CONTENT

Supporting Information

The Supporting Information is available free of charge at https://pubs.acs.org/doi/10.1021/acs.nanolett.0c04640.

Methods regarding proteins, crRNA synthesis, DNA curtain assay, imaging, dynamic light scattering, electrophoretic mobility shift assay, atomic force microscopy, and statistics; figures including results for C−S_{10}−B self-assembly on the DNA and DNA decoration with CRISPR-dCas12a, nucleosomes, and CRISPR-dCas12a-S_{10}; tables with crRNA sequences and parameters for multiple Gaussian fitting (PDF)

Video S1, DNA coating at 25 nM C-S_{10}−B (AVI)

Video S2, DNA coating at 150 nM C-S_{10}−B (AVI)

■ AUTHOR INFORMATION

Corresponding Authors

Ilya J. Finkelstein − *Department of Molecular Biosciences, University of Texas at Austin, Austin, Texas 78712, United States; Institute for Cellular and Molecular Biology and Center for Systems and Synthetic Biology, University of Texas at Austin, Austin, Texas 78712, United States;* orcid.org/0000-0002-9371-2431; Email: armandohg@iquimica.unam.mx

Armando Hernandez-Garcia − *Department of Chemistry of Biomacromolecules, Institute of Chemistry, National Autonomous University of Mexico, Mexico City C.P. 04510, Mexico;* orcid.org/0000-0002-2401-8139; Email: ifinkelstein@cm.utexas.edu

Author

Carlos Calcines-Cruz − *Department of Chemistry of Biomacromolecules, Institute of Chemistry, National Autonomous University of Mexico, Mexico City C.P. 04510, Mexico;* orcid.org/0000-0003-4524-8993

Complete contact information is available at: https://pubs.acs.org/10.1021/acs.nanolett.0c04640

Author Contributions

A.H.G. and I.J.F. conceived the idea for this study and designed the experiments together with C.C.C. C.C.C. performed all the experiments and analyzed the data jointly with I.J.F. and A.H.G. I.J.F., A.H.G., and C.C.C. wrote the manuscript, which was read and approved by all authors.

Notes

The authors declare no competing financial interest.

■ ACKNOWLEDGMENTS

We acknowledge a CONACyT-University of Texas (CONTEX) grant used to carry out this research. A.H.G. also thanks the IA200119 DGAPA-PAPIIT grant. This work was partially funded by the NIH (GM124141 to I.J.F.) and the Welch Foundation (F-1016 to I.J.F.). C.C.C. acknowledges the support of CONACyT for supporting his graduate studies at UT-Austin. We thank David Moreno Gutiérrez for providing some of the C−S_{10}−B protein and all the members of A.H.G.'s and I.J.F.'s laboratories for valuable discussions. We also thank the technicians and appreciate the use of the facilities at the Institute of Chemistry at UNAM, and Tom Wandless at Stanford University for the kind donation of FKBP and FRB plasmids.

■ ABBREVIATIONS

crRNA, CRISPR RNA
FKBP, FK506 binding protein
FRB, FKBP rapamycin binding protein
PAM, protospacer adjacent motif
RNP, ribonucleoprotein particle
VLP, virus-like particle

■ REFERENCES

(1) Hernandez-Garcia, A.; Kraft, D. J.; Janssen, A. F. J.; Bomans, P. H. H.; Sommerdijk, N. A. J. M.; Thies-Weesie, D. M. E.; Favretto, M. E.; Brock, R.; de Wolf, F. A.; Werten, M. W. T.; van der Schoot, P.; Stuart, M. C.; de Vries, R. Design and Self-Assembly of Simple Coat Proteins for Artificial Viruses. *Nat. Nanotechnol.* **2014**, *9* (9), 698−702.

(2) Werten, M. W. T.; Wisselink, W. H.; Jansen-van den Bosch, T. J.; de Bruin, E. C.; de Wolf, F. A. Secreted Production of a Custom-Designed, Highly Hydrophilic Gelatin in Pichia Pastoris. *Protein Eng., Des. Sel.* **2001**, *14* (6), 447−454.

(3) Krejchi, M.; Atkins, E.; Waddon, A.; Fournier, M.; Mason, T.; Tirrell, D. Chemical Sequence Control of *β*-Sheet Assembly in Macromolecular Crystals of Periodic Polypeptides. *Science* **1994**, *265* (5177), 1427−1432.

(4) Smeenk, J. M.; Otten, M. B. J.; Thies, J.; Tirrell, D. A.; Stunnenberg, H. G.; van Hest, J. C. M. Controlled Assembly of Macromolecular *β*-Sheet Fibrils. *Angew. Chem., Int. Ed.* **2005**, *44* (13), 1968−1971.

(5) Zhao, B.; Cohen Stuart, M. A.; Hall, C. K. Dock 'n Roll: Folding of a Silk-Inspired Polypeptide into an Amyloid-like Beta Solenoid. *Soft Matter* **2016**, *12* (16), 3721−3729.

(6) Martin, M. E.; Rice, K. G. Peptide-Guided Gene Delivery. *AAPS J.* **2007**, *9* (1), E18−E29.

(7) Hernandez-Garcia, A.; Werten, M. W. T.; Stuart, M. C.; de Wolf, F. A.; de Vries, R. Coating of Single DNA Molecules by Genetically Engineered Protein Diblock Copolymers. *Small* **2012**, *8* (22), 3491−3501.

(8) Hernandez-Garcia, A.; Cohen Stuart, M. A.; de Vries, R. Templated Co-Assembly into Nanorods of Polyanions and Artificial Virus Capsid Proteins. *Soft Matter* **2018**, *14* (1), 132−139.

(9) Punter, M. T. J. J. M.; Hernandez-Garcia, A.; Kraft, D. J.; de Vries, R.; van der Schoot, P. Self-Assembly Dynamics of Linear Virus-Like Particles: Theory and Experiment. *J. Phys. Chem. B* **2016**, *120* (26), 6286−6297.

(10) Chai, S.; Lurz, R.; Alonso, J. C. The Small Subunit of the Terminase Enzyme of Bacillus Subtilis Bacteriophage SPP1 Forms a Specialized Nucleoprotein Complex with the Packaging Initiation Region. *J. Mol. Biol.* **1995**, *252* (4), 386−398.

(11) Turner, D. R.; Joyce, L. E.; Butler, P. J. G. The Tobacco Mosaic Virus Assembly Origin RNA. *J. Mol. Biol.* **1988**, *203* (3), 531−547.

(12) D'Souza, V.; Melamed, J.; Habib, D.; Pullen, K.; Wallace, K.; Summers, M. F. Identification of a High Affinity Nucleocapsid Protein Binding Element within the Moloney Murine Leukemia Virus Ψ-RNA Packaging Signal: Implications for Genome Recognition. *J. Mol. Biol.* **2001**, *314* (2), 217−232.

(13) de Beer, T.; Fang, J.; Ortega, M.; Yang, Q.; Maes, L.; Duffy, C.; Berton, N.; Sippy, J.; Overduin, M.; Feiss, M.; Catalano, C. E. Insights into Specific DNA Recognition during the Assembly of a Viral Genome Packaging Machine. *Mol. Cell* **2002**, *9* (5), 981−991.

(14) Borodavka, A.; Tuma, R.; Stockley, P. G. Evidence That Viral RNAs Have Evolved for Efficient, Two-Stage Packaging. *Proc. Natl. Acad. Sci. U. S. A.* **2012**, *109* (39), 15769−15774.

(15) Kutluay, S. B.; Zang, T.; Blanco-Melo, D.; Powell, C.; Jannain, D.; Errando, M.; Bieniasz, P. D. Global Changes in the RNA Binding

Specificity of HIV-1 Gag Regulate Virion Genesis. *Cell* **2014**, *159* (5), 1096−1109.
(16) Stewart, H.; Bingham, R. J.; White, S. J.; Dykeman, E. C.; Zothner, C.; Tuplin, A. K.; Stockley, P. G.; Twarock, R.; Harris, M. Identification of Novel RNA Secondary Structures within the Hepatitis C Virus Genome Reveals a Cooperative Involvement in Genome Packaging. *Sci. Rep.* **2016**, *6* (1), 22952.
(17) Patel, N.; Wroblewski, E.; Leonov, G.; Phillips, S. E. V.; Tuma, R.; Twarock, R.; Stockley, P. G. Rewriting Nature's Assembly Manual for a ssRNA Virus. *Proc. Natl. Acad. Sci. U. S. A.* **2017**, *114* (46), 12255−12260.
(18) Morton, V. L.; Dykeman, E. C.; Stonehouse, N. J.; Ashcroft, A. E.; Twarock, R.; Stockley, P. G. The Impact of Viral RNA on Assembly Pathway Selection. *J. Mol. Biol.* **2010**, *401* (2), 298−308.
(19) Kraft, D. J.; Kegel, W. K.; van der Schoot, P. A Kinetic Zipper Model and the Assembly of Tobacco Mosaic Virus. *Biophys. J.* **2012**, *102* (12), 2845−2855.
(20) Comas-Garcia, M.; Datta, S. A.; Baker, L.; Varma, R.; Gudla, P. R.; Rein, A. Dissection of Specific Binding of HIV-1 Gag to the "packaging Signal" in Viral RNA. *eLife* **2017**, *6*, No. e27055.
(21) Comas-Garcia, M. Packaging of Genomic RNA in Positive-Sense Single-Stranded RNA Viruses: A Complex Story. *Viruses* **2019**, *11* (3), 253.
(22) Strohkendl, I.; Saifuddin, F. A.; Rybarski, J. R.; Finkelstein, I. J.; Russell, R. Kinetic Basis for DNA Target Specificity of CRISPR-Cas12a. *Mol. Cell* **2018**, *71* (5), 816−824.e3.
(23) Zetsche, B.; Heidenreich, M.; Mohanraju, P.; Fedorova, I.; Kneppers, J.; DeGennaro, E. M.; Winblad, N.; Choudhury, S. R.; Abudayyeh, O. O.; Gootenberg, J. S.; Wu, W. Y.; Scott, D. A.; Severinov, K.; van der Oost, J.; Zhang, F. Multiplex Gene Editing by CRISPR−Cpf1 Using a Single CrRNA Array. *Nat. Biotechnol.* **2017**, *35* (1), 31−34.
(24) Gallardo, I. F.; Pasupathy, P.; Brown, M.; Manhart, C. M.; Neikirk, D. P.; Alani, E.; Finkelstein, I. J. High-Throughput Universal DNA Curtain Arrays for Single-Molecule Fluorescence Imaging. *Langmuir* **2015**, *31* (37), 10310−10317.
(25) Soniat, M. M.; Myler, L. R.; Schaub, J. M.; Kim, Y.; Gallardo, I. F.; Finkelstein, I. J. Next-Generation DNA Curtains for Single-Molecule Studies of Homologous Recombination. *Methods Enzymol.* **2017**, *592*, 259−281.
(26) Miné, J.; Disseau, L.; Takahashi, M.; Cappello, G.; Dutreix, M.; Viovy, J.-L. Real-Time Measurements of the Nucleation, Growth and Dissociation of Single Rad51−DNA Nucleoprotein Filaments. *Nucleic Acids Res.* **2007**, *35* (21), 7171−7187.
(27) Marchetti, M.; Kamsma, D.; Cazares Vargas, E.; Hernandez García, A.; van der Schoot, P.; de Vries, R.; Wuite, G. J. L.; Roos, W. H. Real-Time Assembly of Viruslike Nucleocapsids Elucidated at the Single-Particle Level. *Nano Lett.* **2019**, *19* (8), 5746−5753.
(28) Gao, L.; Cox, D. B. T.; Yan, W. X.; Manteiga, J. C.; Schneider, M. W.; Yamano, T.; Nishimasu, H.; Nureki, O.; Crosetto, N.; Zhang, F. Engineered Cpf1 Variants with Altered PAM Specificities Increase Genome Targeting Range. *Nat. Biotechnol.* **2017**, *35* (8), 789−792.
(29) Leenay, R. T.; Beisel, C. L. Deciphering, Communicating, and Engineering the CRISPR PAM. *J. Mol. Biol.* **2017**, *429* (2), 177−191.
(30) Nishimasu, H.; Shi, X.; Ishiguro, S.; Gao, L.; Hirano, S.; Okazaki, S.; Noda, T.; Abudayyeh, O. O.; Gootenberg, J. S.; Mori, H.; Oura, S.; Holmes, B.; Tanaka, M.; Seki, M.; Hirano, H.; Aburatani, H.; Ishitani, R.; Ikawa, M.; Yachie, N.; Zhang, F.; Nureki, O. Engineered CRISPR-Cas9 Nuclease with Expanded Targeting Space. *Science* **2018**, *361* (6408), 1259−1262.
(31) Walton, R. T.; Christie, K. A.; Whittaker, M. N.; Kleinstiver, B. P. Unconstrained Genome Targeting with Near-PAMless Engineered CRISPR-Cas9 Variants. *Science* **2020**, *368* (6488), 290−296.

https://doi.org/10.1021/acs.nanolett.0c04640
Nano Lett. XXXX, XXX, XXX−XXX